Electronic Supplementary Information

Synchronous Nesting of Hollow FeP Nanospheres into Three-dimensional Porous Carbon Scaffold *via* Salt-template Method for Performance-enhanced Potassium-ion Storage

Qiwei Tan,‡[a] Kun Han,‡[a] Wang Zhao,[a] Ping Li,*[a] Zhiwei Liu,[b] Shengwei Li[a] and Xuanhui Qu[a]

[a] *Beijing Advanced Innovation Center for Materials Genome Engineering, Institute for Advanced Materials and Technology, University of Science and Technology Beijing, Beijing 100083, China.*

Email: ustbliping@126.com

[b] *College of Materials Science and Engineering, Key Laboratory of Advanced Functional Materials, Education Ministry of China, Beijing University of Technology, Beijing 100124, P.R. China.*

‡ Q. Tan and K. Han contributed equally to this work.

$$FeCl_3 + C_6H_8O_7 \cdot H_2O \rightarrow Fe_3O_4 + C + HCl \uparrow + H_2O \uparrow + CO/CO_2 \uparrow$$

$$PVP \rightarrow \textbf{N-doped Carbon} + CO/CO_2 \uparrow + H_2O \uparrow$$

Note S1 Chemical reactions involved in the formation process of the Fe_3O_4@3D-PC@NaCl during calcination.

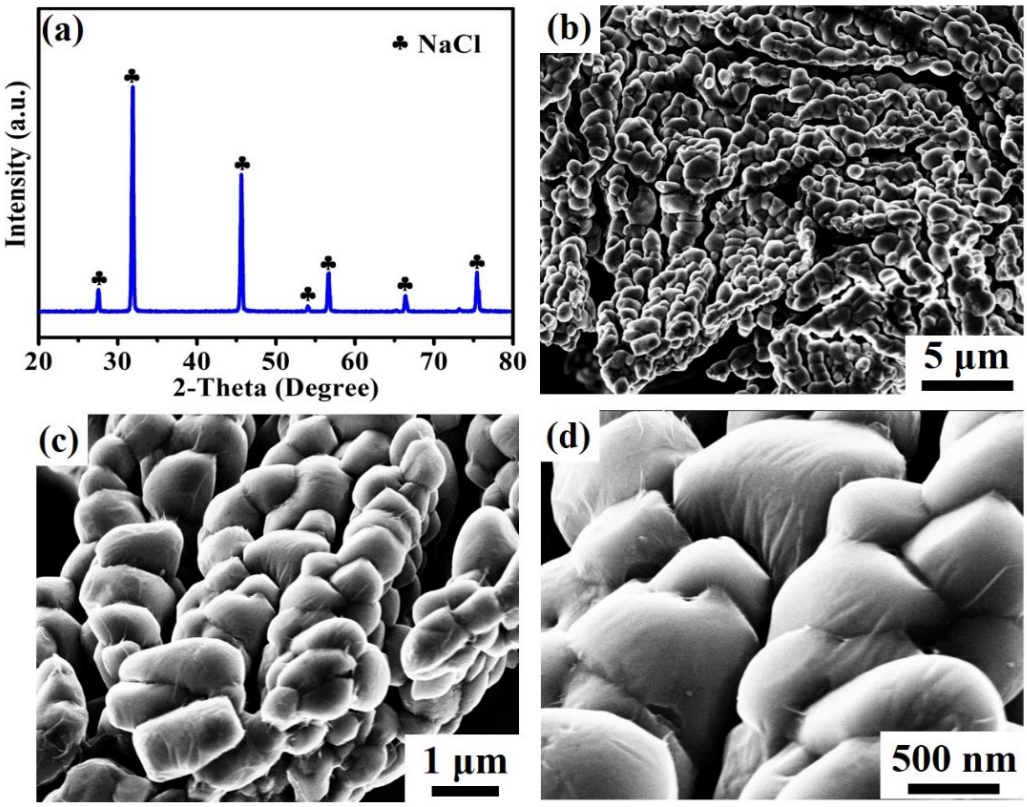

Fig. S1 (a) XRD pattern and (b-d) FESEM micrographs of the Fe_3O_4@3D-PC@NaCl precursor obtained after calcination at 700 °C for 2 h in Ar atmosphere.

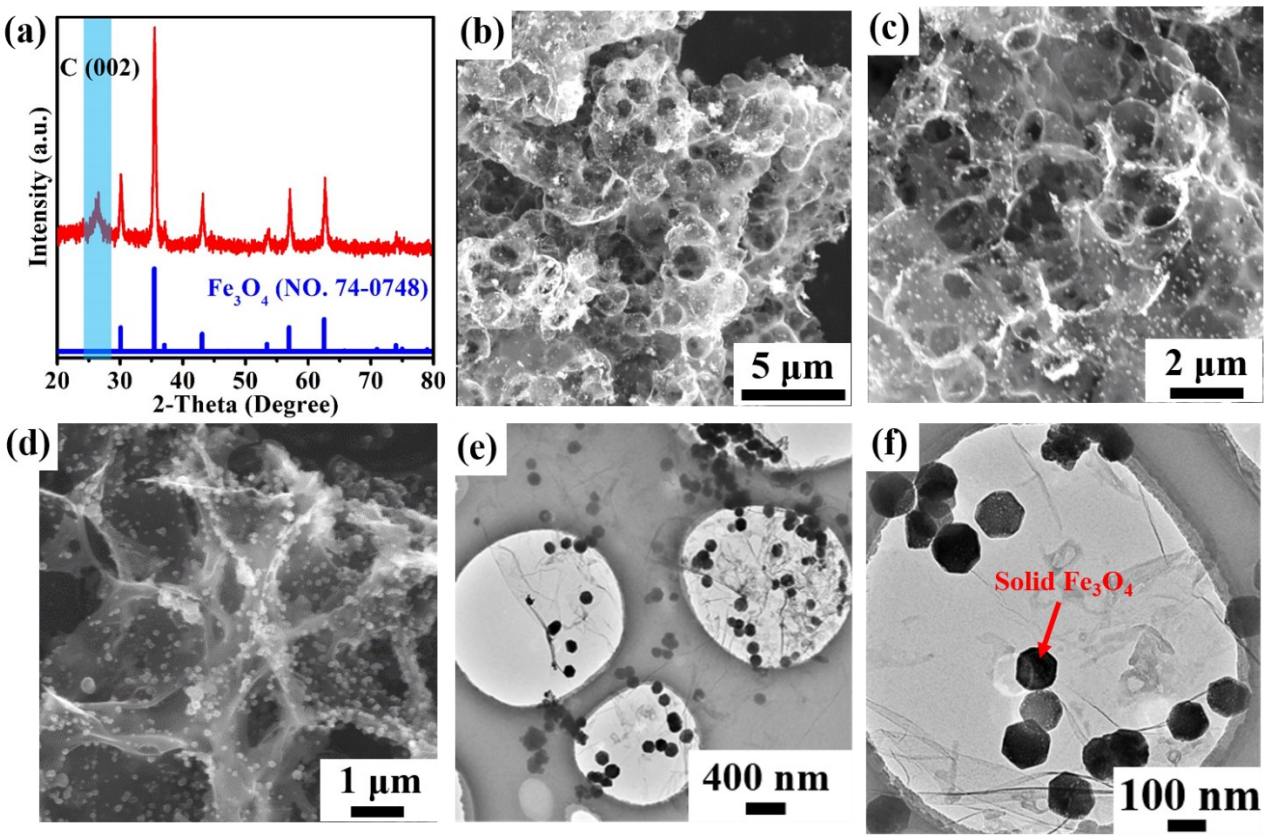

Fig. S2 (a) XRD pattern, (b-d) FESEM and (e, f) TEM micrographs of the Fe_3O_4@3D-PC precursor.

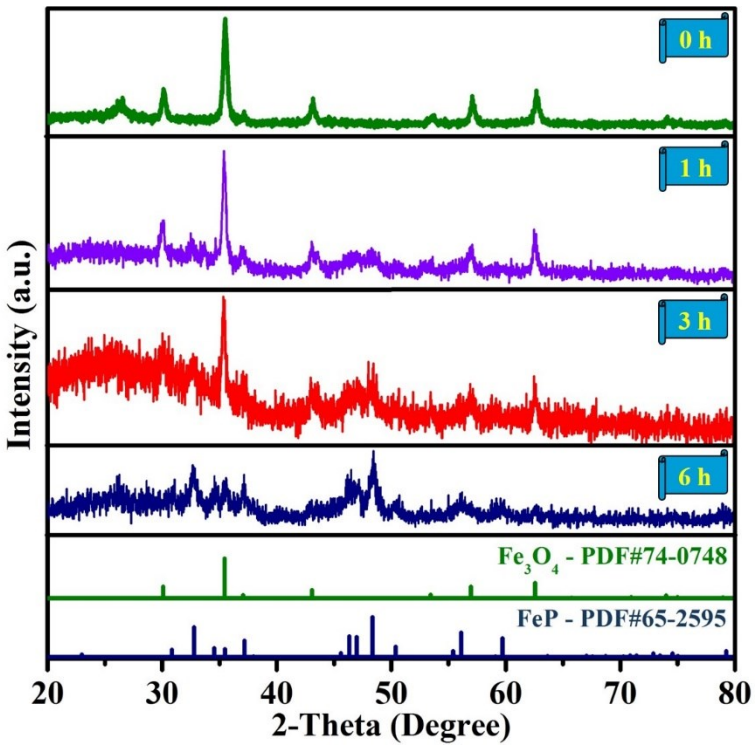

Fig. S3 XRD patterns of the Fe_3O_4@3D-PC precursor before (0 h) and after phosphorization treatment at 360 °C for 1 h, 3h and 6 h, respectively.

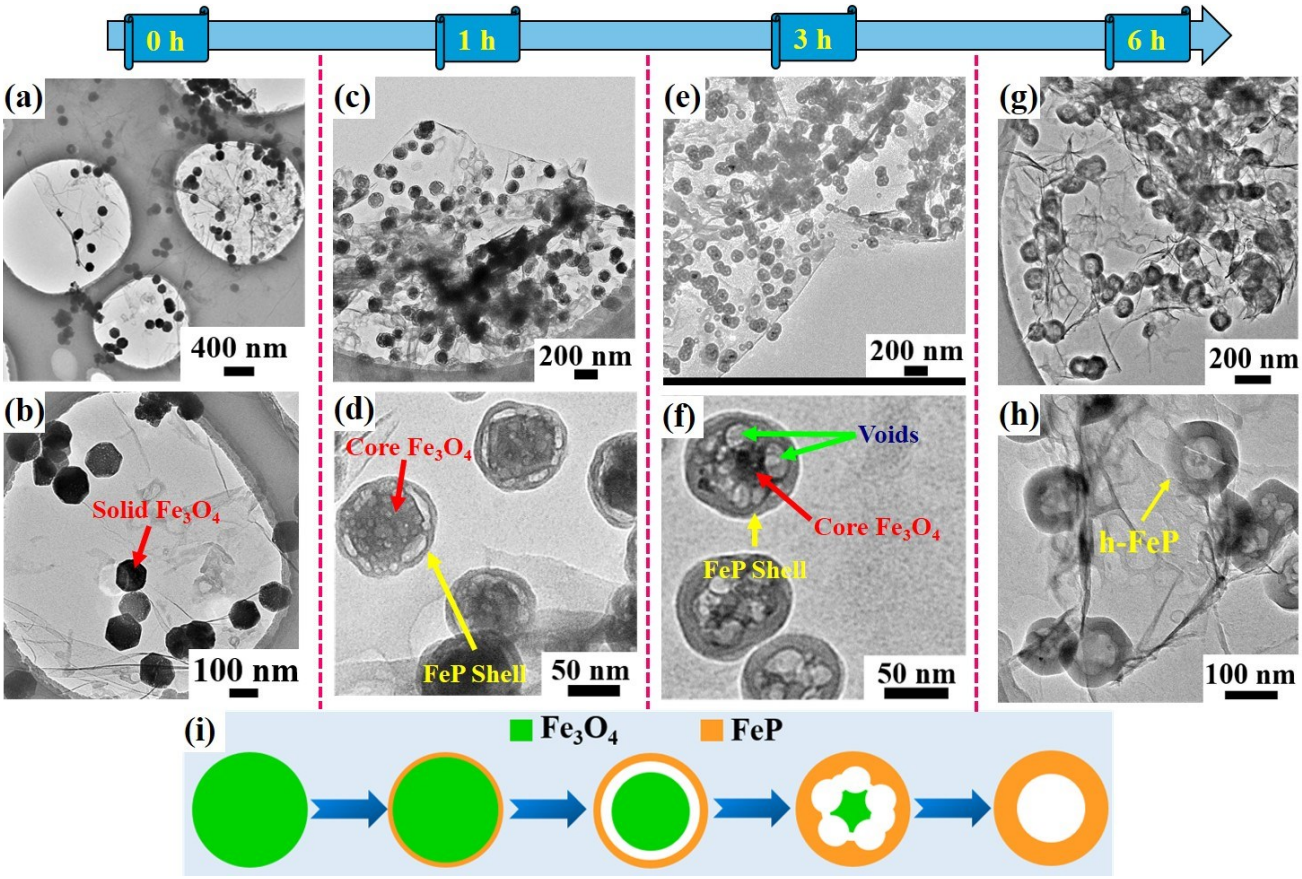

Fig. S4 TEM micrographs of the Fe_3O_4@3D-PC precursor (a, b) before (0 h) and after phosphorization treatment at 360 °C for (c, d) 1 h, (e, f) 3 h and (g, h) 6 h, respectively. (i) The schematic illlustration of the transformation process of the Fe_3O_4@3D-PC precursor to the h-FeP@3D-PC.

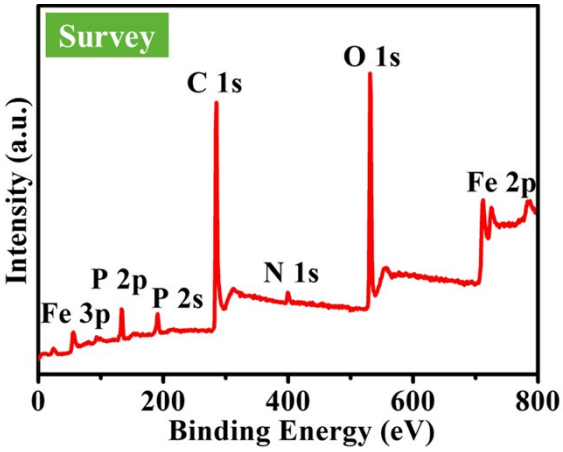

Fig. S5 (a) XPS survey profile of the FeP@3D-PC.

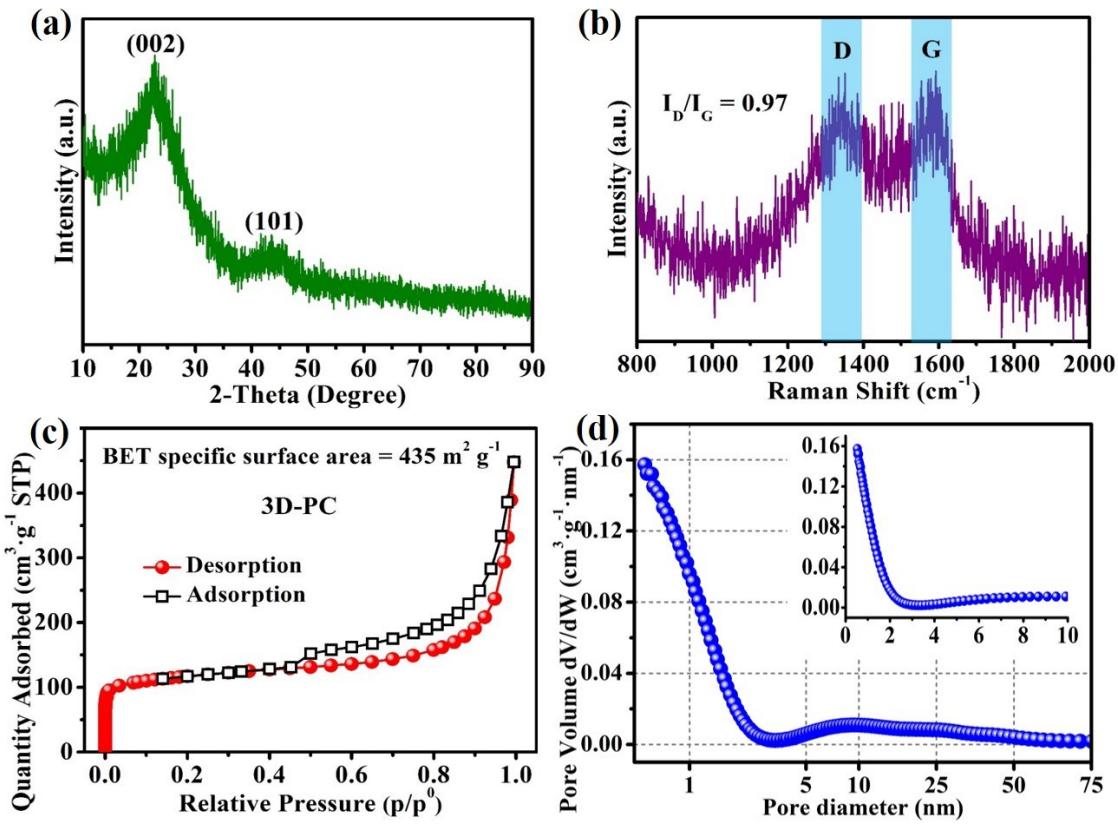

Fig. S6 (a) XRD pattern, (b) Raman spectrum, (c) N_2 adsorption-desorption profile and (e-f) Pore size distribution profile of the 3D-PC.

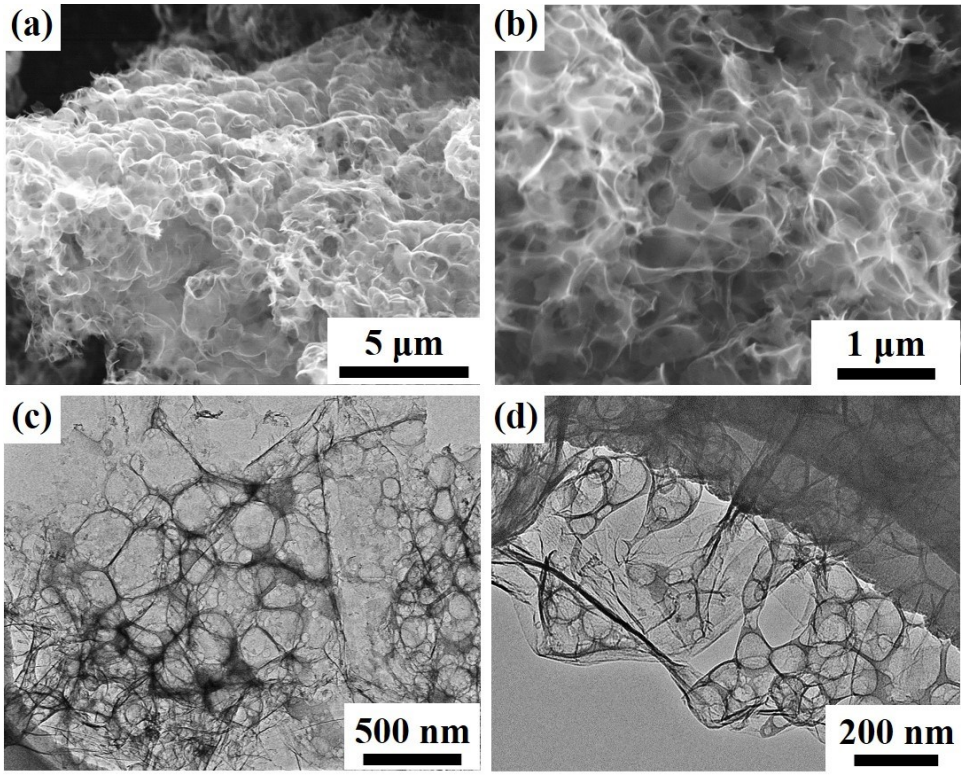

Fig. S7 (a-b) FESEM and (c-d) TEM images of the 3D-PC.

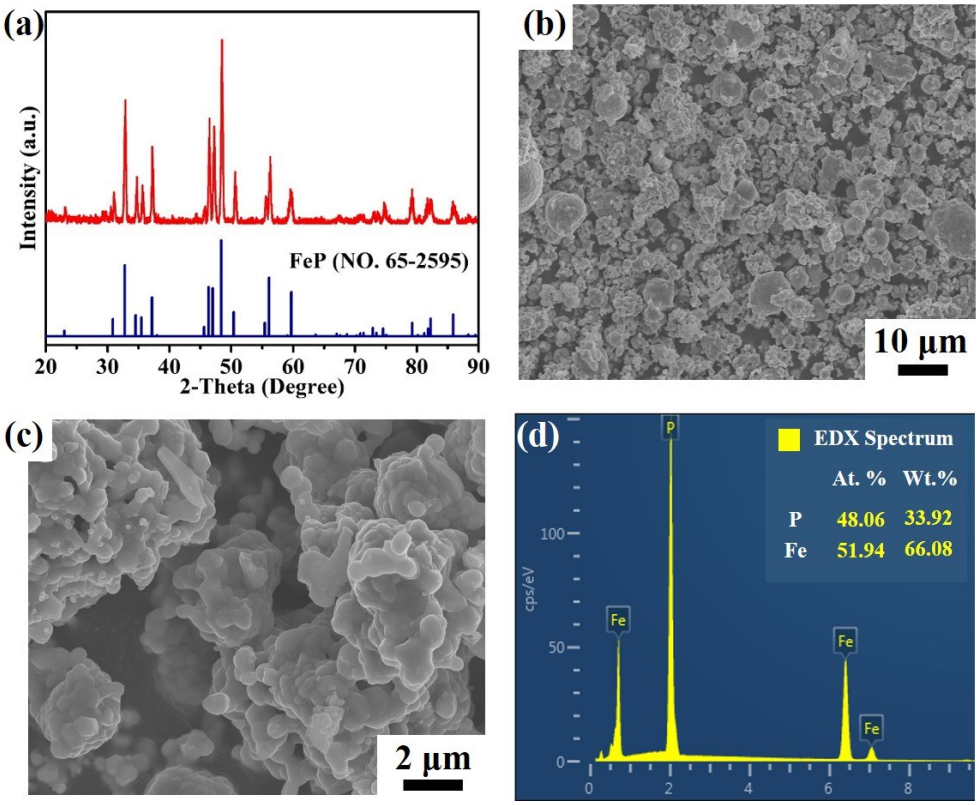

Fig. S8 (a) XRD pattern of the s-FeP. (b-c) FESEM images and (d) EDX spectrum of the s-FeP.

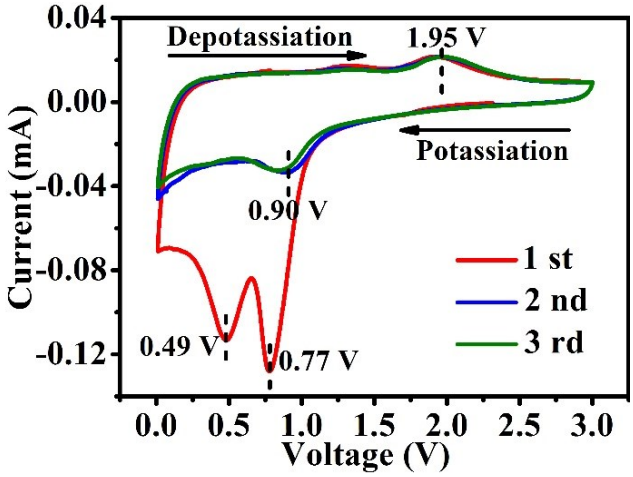

Fig. S9 Cyclic voltammetry profiles of the h-FeP@3D-PC recorded at a scan rate of 0.1 mV s^{-1} for the first three cycles.

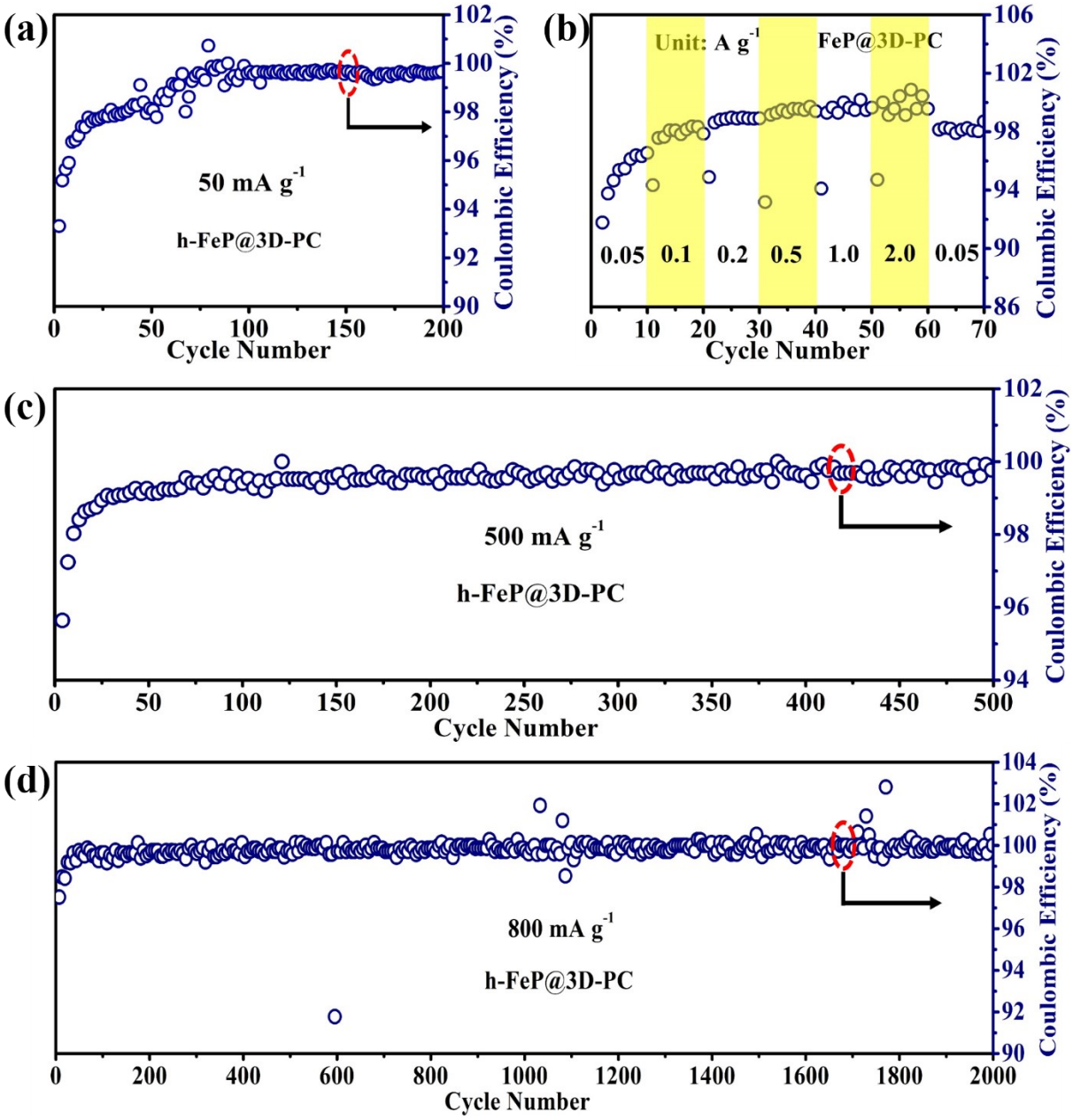

Fig. S10 Independent plots of Coulombic efficiency *vesus* cycle number of the h-FeP@3D-PC tested at current density of (a) 50 mA g^{-1}. (b) various current densities from 0.5 to 2 A g^{-1}. (c) 500 mA g^{-1} and (d) 800 mA g^{-1}.

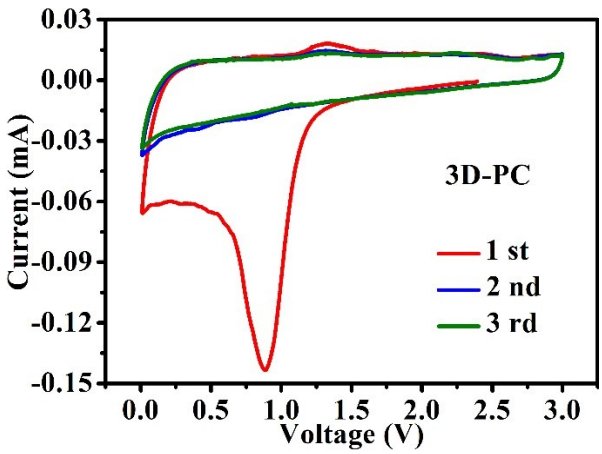

Fig. S11 Cyclic voltammetry profiles of the 3D-PC electrode recorded at a scan rate of 0.1 mV s^{-1} for the first three cycles.

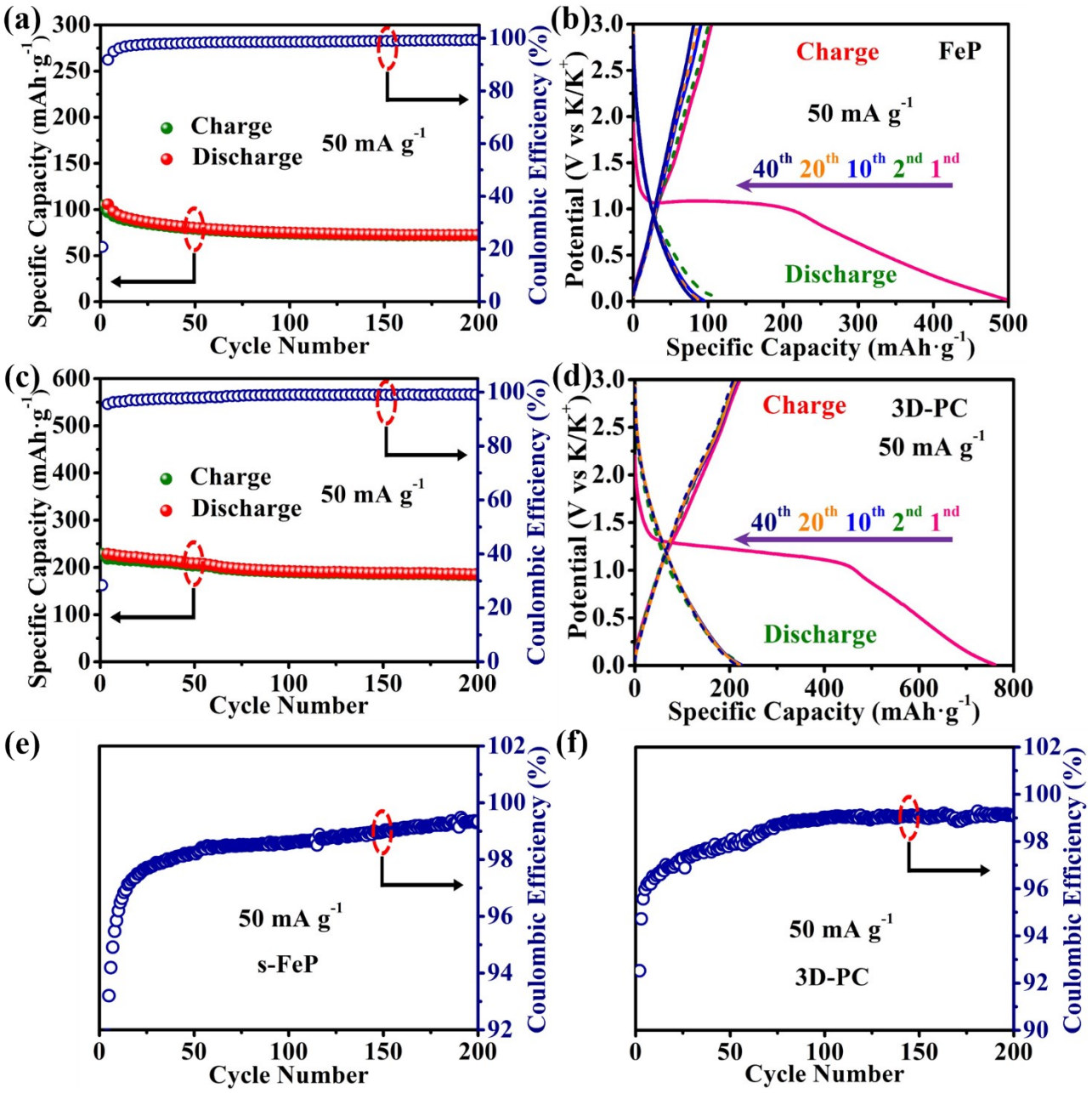

Fig. S12 (a) Charge-discharge tests and (b) the corresponding potential *vs.* specific capacity curves of the s-FeP electrode tested at 50 mA g^{-1} for 200 cycles. (c) Charge-discharge tests and (d) the corresponding potential *vs.* specific capacity curves of the 3D-PC electrode tested at 50 mA g^{-1} for 200 cycles. Enlarged Coulombic efficiency versus cycle number plots of (e) s-FeP and (f) 3D-PC electrodes.

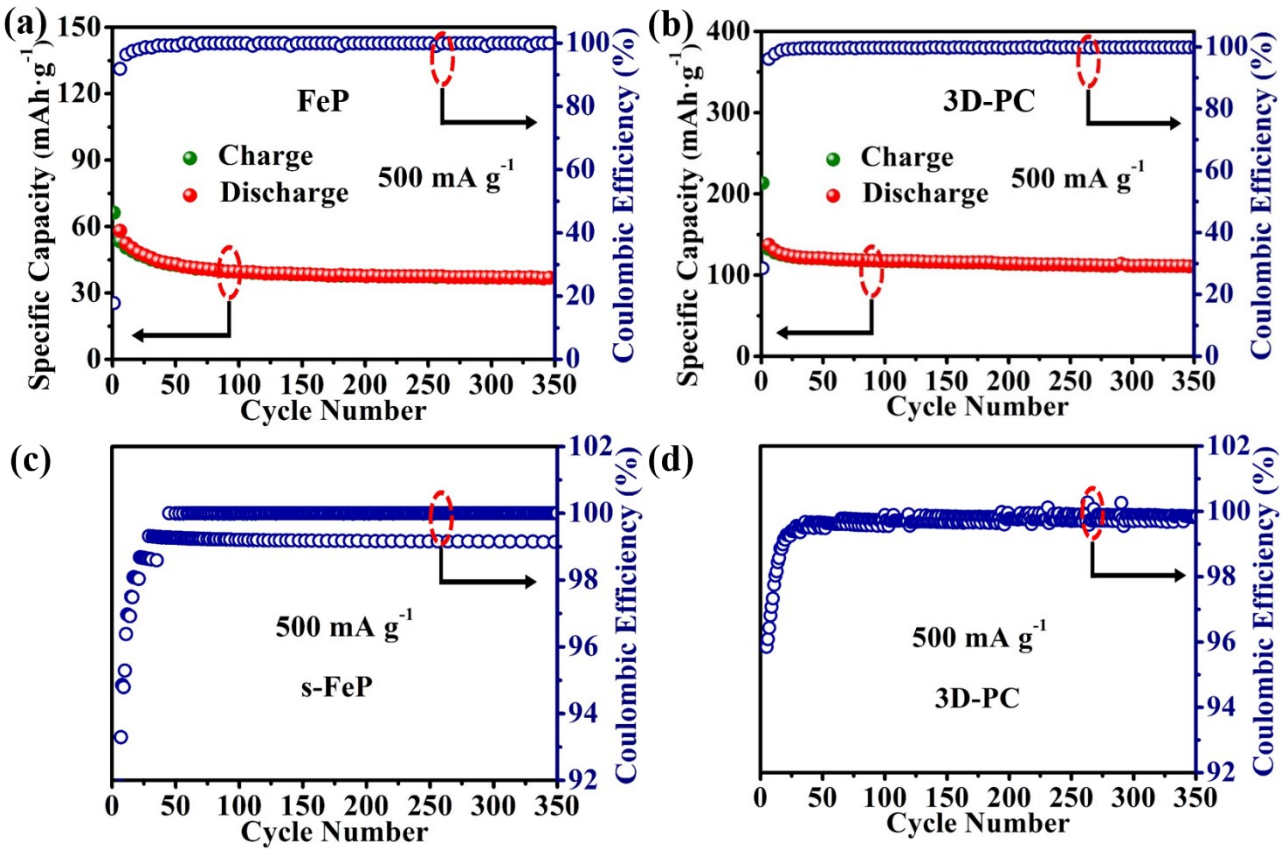

Fig. S13 Cycling performance of (a) the s-FeP and (b) the 3D-PC electrodes for potassium storage. Enlarged Coulombic efficiency versus cycle number plots of (c) s-FeP and (d) 3D-PC electrodes.

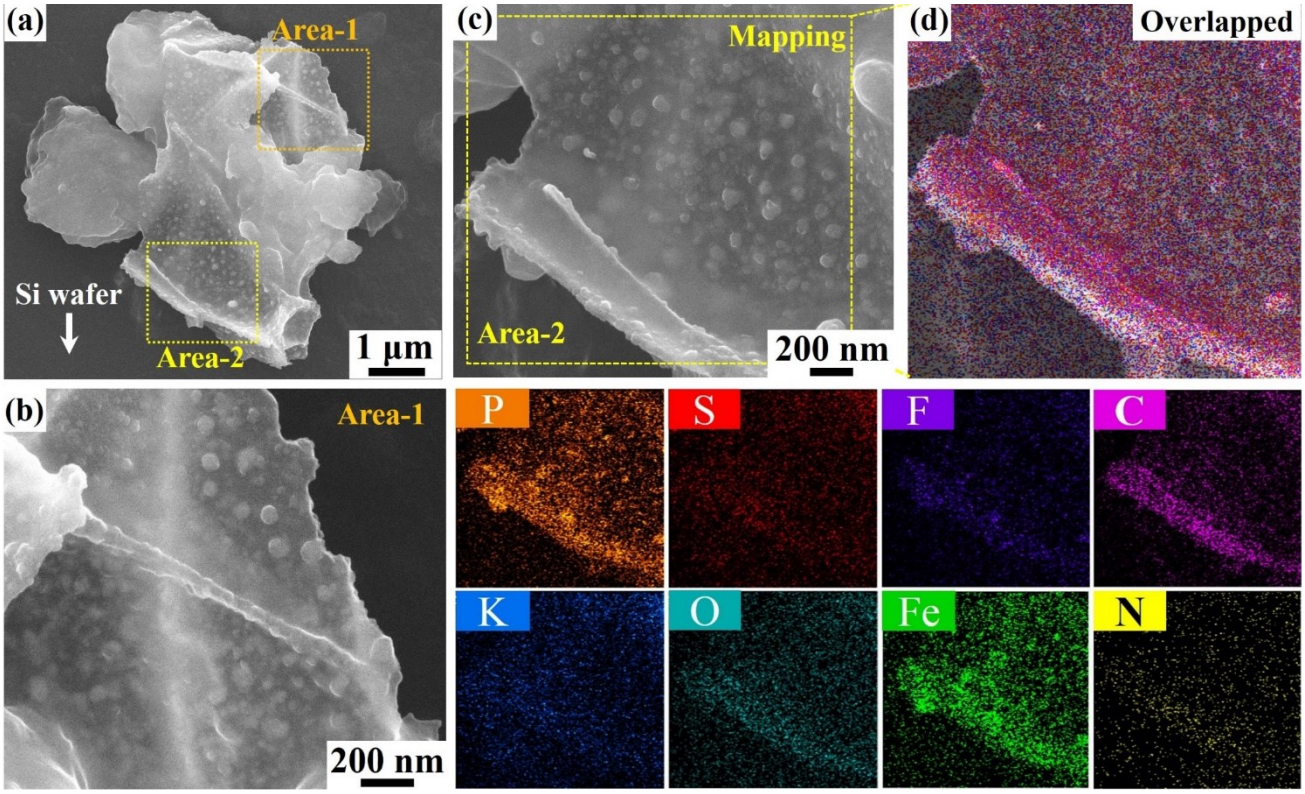

Fig. S14 (a-c) *Ex-situ* FESEM micrographs of the h-FeP@3D-PC electrode after cycled at 50 mA g^{-1} for 40 cycles and (c) Corresponding elemental mapping images of the overlapped and P, S, F, C, K, O, Fe and N, respectively.

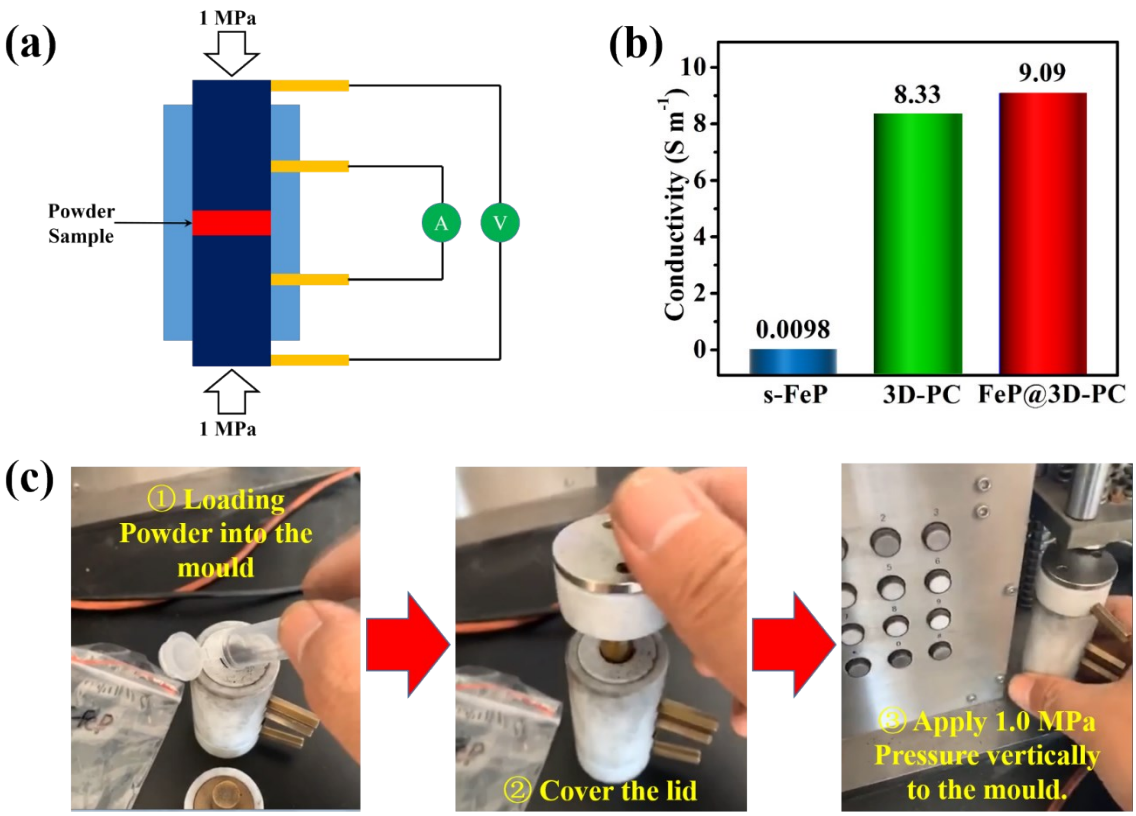

Fig. S15 (a) Schematic diagram of the mould for powder conductivity measurement, (b) Conductivity results of s-FeP, 3D-PC and h-FeP@3D-PC materials, respectively and (c) Digital photos of three steps to load the powder sample into the mould and apply vertical pressure to the powder.

In a typical procedure, a mould was utilized to hold the powder sample for conductivity measurement tests. Firstly, the powder sample was loaded into the mould, and the upper lid was covered after that. Subsequently, the mould was placed inside a hydraulic machine, and 1.0 MPa external pressure was applied vertically to the mould, therefore, the powder can be pressed as a disk inside the mould, and the conductivity of the powder sample can be measured and recorded simultaneously.

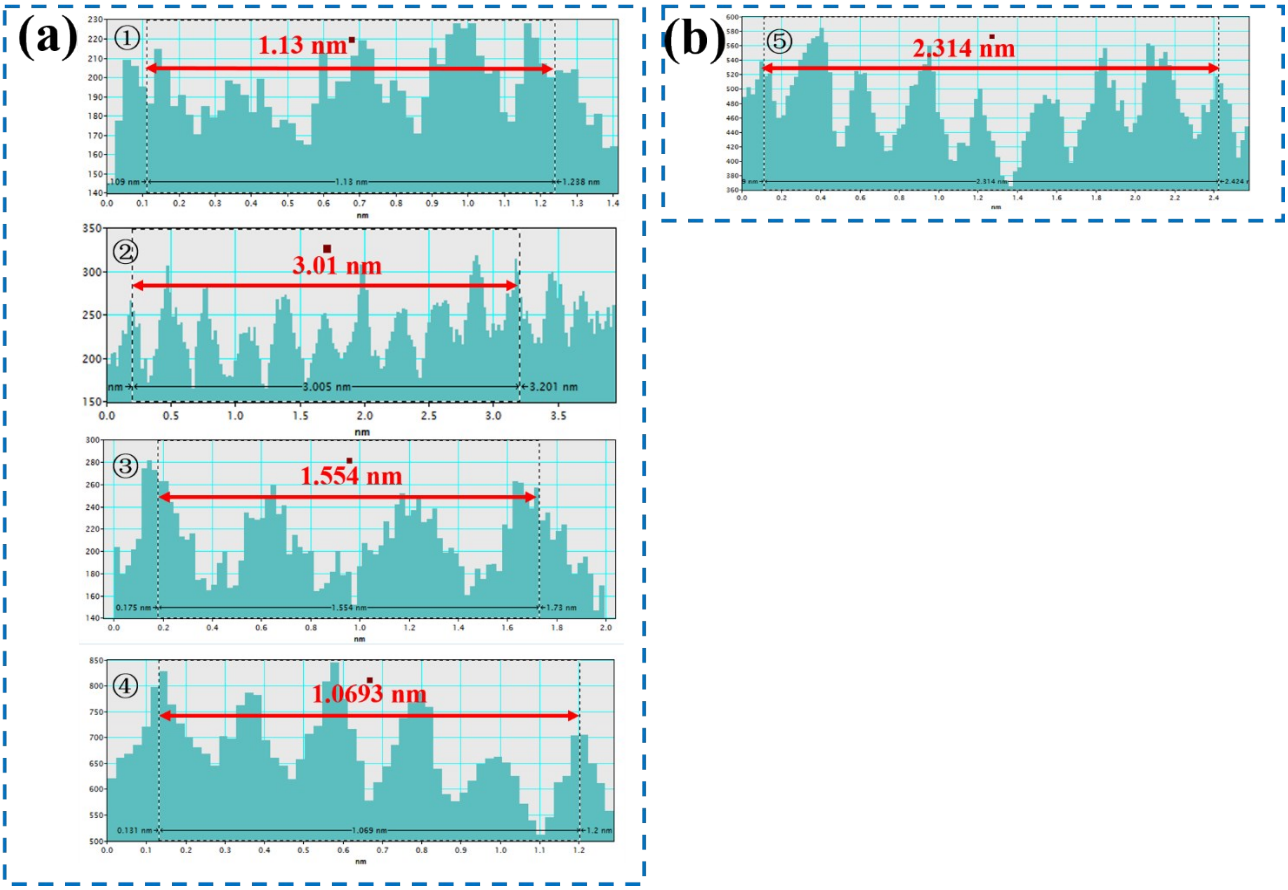

Fig. S16 The corresponding lattice fringe images of the h-FeP@3D-PC material after (a) fully discharged to 0.01 V and (b) Charged to 3.0 V.

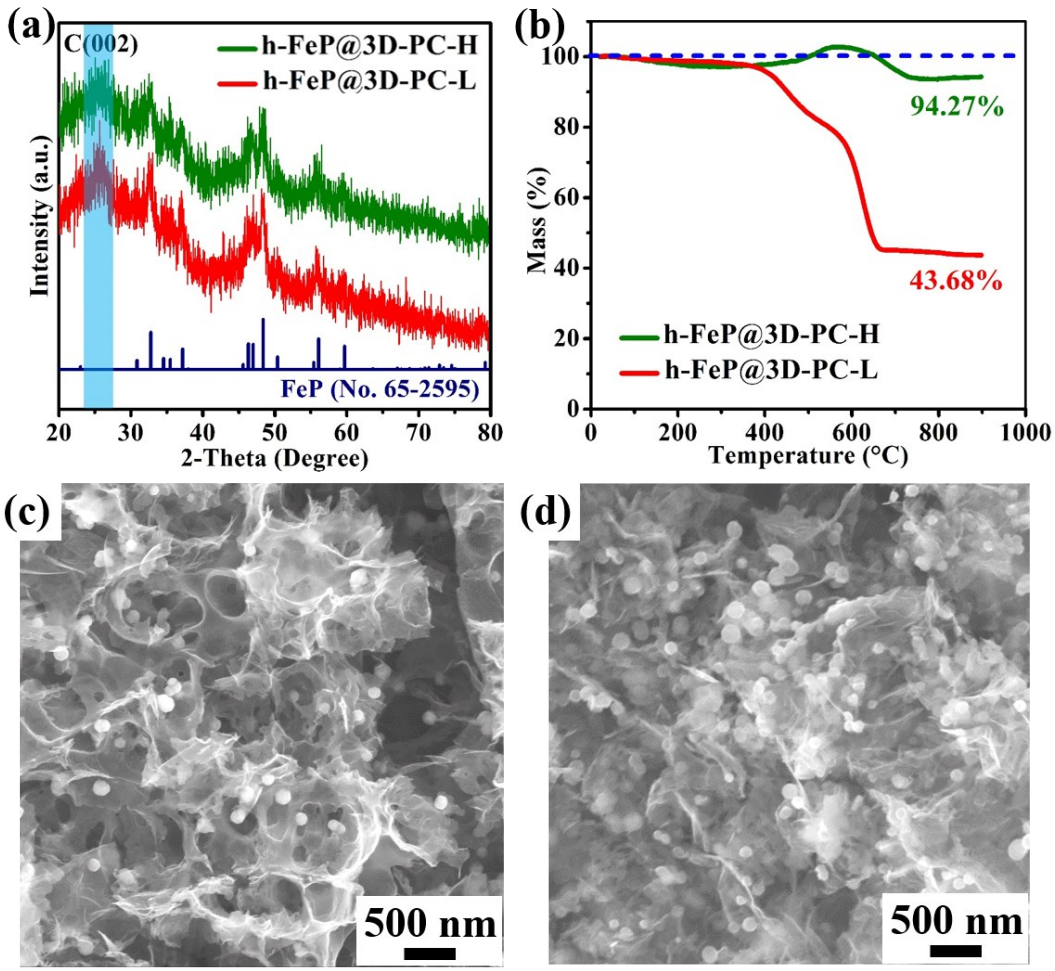

Fig. S17 (a) XRD patterns and (b) TGA plots of h-FeP@3D-PC-L and h-FeP@3D-PC-H. FESEM micrographs of (c) h-FeP@3D-PC-L and (d) h-FeP@3D-PC-H.

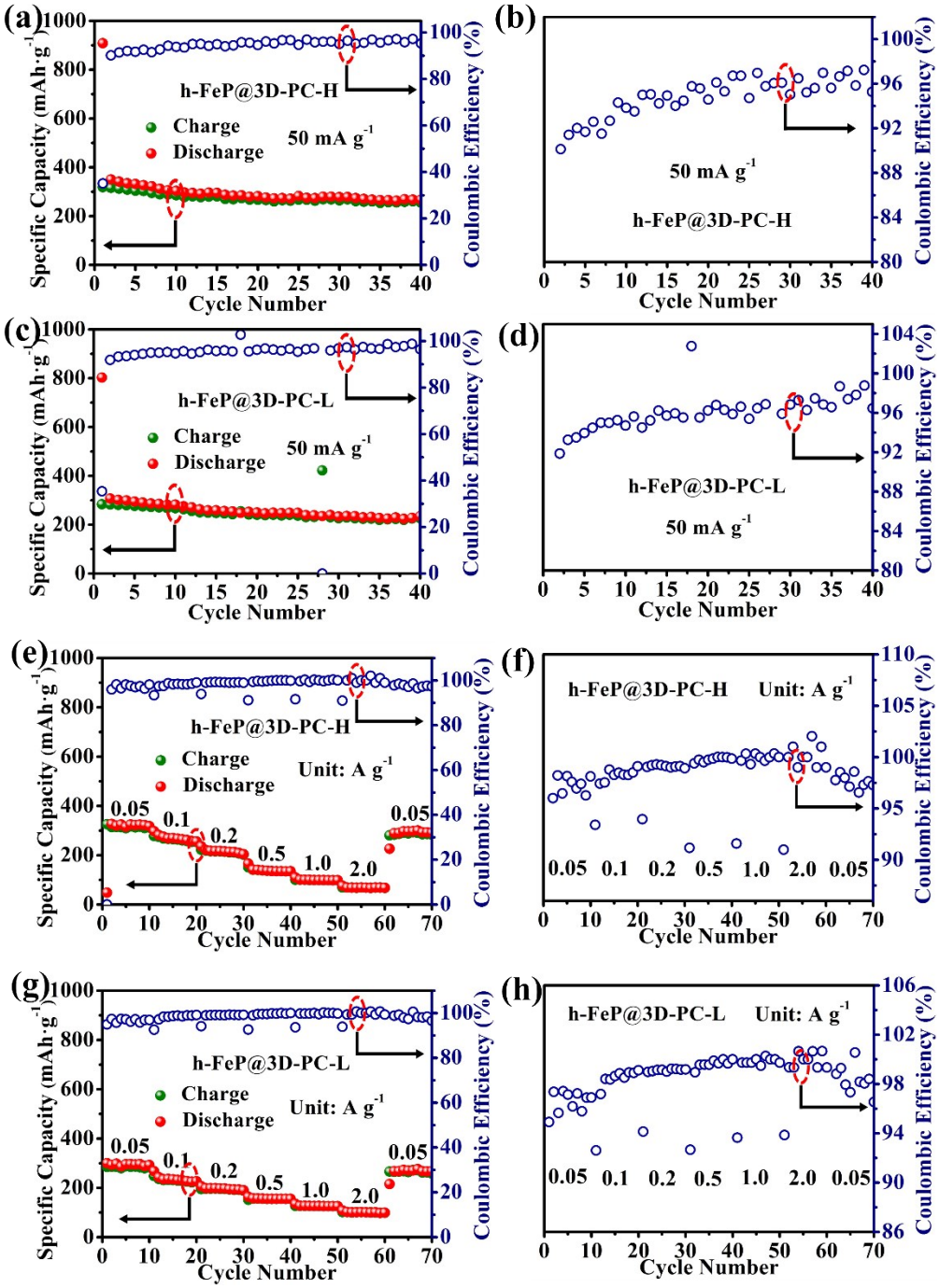

Fig. S18 Charge-discharge tests of (a) h-FeP@3D-PC-H and (c) h-FeP@3D-PC-L performed at 50 mA g^{-1}. Rate capabilities of (e) h-FeP@3D-PC-H and (g) h-FeP@3D-PC-L measured under various current densities from 0.05~2.0 A g^{-1}. The corresponding enlarged Coulombic efficiency *vesus* cycle number of (b) h-FeP@3D-PC-H and (d) h-FeP@3D-PC-L performed at 50 mA g^{-1}. Rate capabilities of (f) h-FeP@3D-PC-H and (h) h-FeP@3D-PC-L measured under various current densities from 0.05~2.0 A g^{-1}.

Table S1 A comparative list of some representative anode materials for potassium-ion batteries.

Anode Materials	Current density (mA g^{-1})	Manifest capacity (mAh g^{-1})	Cycle Stability (Retention/cycles/Rate)	Ref.
h-FeP@3D-PC	**50**	**343.5**	**178 mAh g^{-1}/500/0.5 A g^{-1}**	**This work**
	1000	**171.3**		
	2000	**140.2**		
FeP/C	50	288.9	183 mAh g^{-1}/50/0.05 A g^{-1}	[1]
	1000	78.7		
YS-FeP@CNBs	100	264	205 mAh g^{-1}/300/0.1 A g^{-1}	[2]
	2000	37		
CoP⊂NPPCS	50	174	114 mAh g^{-1}/1000/0.5 A g^{-1}	[3]
	2000	54		
FeS_2@RGO	50	351	123 mAh g^{-1}/420/0.5 A g^{-1}	[4]
	500	151		
$SnP_{0.94}$@rGO	25	294	106 mAh g^{-1}/100/0.2 A g^{-1}	[5]
	1000	57		
Black P-C	200	210	270 mAh g^{-1}/50/0.05 A g^{-1}	[6]
	500	120		
$K_{0.6}Mn_1F_{2.7}$	20	182	110 mAh g^{-1}/10000/0.4 A g^{-1}	[7]
	1000	78		

ZnS@C@rGO	100	362	208 mAh g^{-1}/300/0.5 A g^{-1}	[8]
	500	162		
HPC	50	211.5	90.1 mAh g^{-1}/1000/1 A g^{-1}	[9]
	10000	76.7		
Sn_4P_3/RGO	100	282	156 mAh g^{-1}/60/0.6 A g^{-1}	[10]
	1000	67		
$K_2Ti_4O_9$	30	97	40 mAh g^{-1}/30/0.1 A g^{-1}	[11]
	100	80		
OMC	50	286.4	146.5 mAh g^{-1}/1000/1 A g^{-1}	[12]
	1000	144.2		

Table S2 A list of potassiation products of metal phoshide/phosphorus anode materials for KIBs reported in literatures.

Anode Materials	**Potassiation Products**	**Investigation Methods**	**Ref.**
FeP/C	Fe + K_3P	*ex-situ* XRD	[1]
$SnP_{0.94}$@rGO	KSn + $K_{3-x}P$	*ex-situ* XRD	[5]
Black P-C	KP	*ex-situ* XRD	[6]
Sn_4P_3@C	KSn + $K_{3-x}P$	*ex-situ* XRD, *ex-situ* HRTEM, SAED	[13]
Sn_4P_3@CNFs	KSn + K_3P	In operando synchrotron XRD, *ex-situ* HRTEM, SAED	[14]
AC@CoP/NCNTs/CNFs	Co + K_3P	*ex-situ* XRD, *ex-situ* HRTEM	[15]
3DG/FeP	Fe + K_3P	*ex-situ* XRD, *ex-situ* HRTEM	[16]
P/C	KP	*ex-situ* XRD	[17]
Sn_4P_3/C	KSn + K_3P	*ex-situ* XRD, *ex-situ* HRTEM, SAED	[18]
Red P/C	KP	*ex-situ* XRD	[19]
Red P@N-PHCNFs	K_4P_3	*ex-situ* XRD	[20]
Red P@CN	KP	*ex-situ* XRD, *ex-situ* HRTEM, SAED, DFT calculations	[21]
GeP_5	GeK + K_4P_3	In operando synchrotron XRD	[22]
NC@CoP/NC	Co + K_3P	*ex-situ* XRD, *ex-situ* HRTEM, SAED	[23]
PNR/C	K_4P_3	dQ/dVplots and related analysis	[24]

References

1. W. Li, B. Yan, H. Fan, C. Zhang, H. Xu, X. Cheng, Z. Li, G. Jia, S. An and X. Qiu, *ACS Appl. Mater. Inter.*, 2019, **11**, 22364-22370.
2. F. Yang, H. Gao, J. Hao, S. Zhang, P. Li, Y. Liu, J. Chen and Z. Guo, *Adv. Funct. Mater.*, 2019, **29**, 1808291.
3. J. Bai, B. Xi, H. Mao, Y. Lin, X. Ma, J. Feng and S. Xiong, *Adv. Mater.*, 2018, **30**, 1802310.
4. J. Xie, Y. Zhu, N. Zhuang, H. Lei, W. Zhu, Y. Fu, M. S. Javed, J. Li and W. Mai, *Nanoscale*, 2018, **10**, 17092-17098.
5. X. Zhao, W. Wang, Z. Hou, G. Wei, Y. Yu, J. Zhang and Z. Quan, *Chem. Eng. J.*, 2019, **370**, 677-683.
6. I. Sultana, M. M. Rahman, T. Ramireddy, Y. Chen and A. M. Glushenkov, *J. Mater. Chem. A*, 2017, **5**, 23506-23512.
7. Z. Liu, P. Li, G. Suo, S. Gong, W. A. Wang, C. Lao, Y. Xie, H. Guo, Q. Yu, W. Zhao, K. Han, Q. Wang, M. Qin, K. Xi and X. Qu, *Energ. Environ. Sci.*, 2018, **11**, 3033-3042.
8. J. Chu, W. Wang, J. Feng, C. Lao, K. Xi, L. Xing, K. Han, Q. Li, L. Song, P. Li, X. Li and Y. Bao, *ACS Nano*, 2019, **13**, 6906-6916.
9. X. Wu, C. W. K. Lam, N. Wu, S. Pang, Z. Xing, W. Zhang and Z. Ju, *Materials Today Energy*, 2019, **11**, 182-191.
10. W. Yang, J. Zhang, D. Huo, S. Sun, S. Tao, Z. Wang, J. Wang, D. Wu and B. Qian, *Ionics*, 2019, **25**, 4795-4803.
11. B. Kishore, V. G and N. Munichandraiah, *J. Electrochem. Soc.*, 2016, **163**, A2551-A2554.
12. W. Wang, J. Zhou, Z. Wang, L. Zhao, P. Li, Y. Yang, C. Yang, H. Huang and S. Guo, *Adv.*

Energy Mater., 2018, **8**, 1701648.

13. D. Li, Y. Zhang, Q. Sun, S. Zhang, Z. Wang, Z. Liang, P. Si and L. Ci, *Energy Storage Materials*, 2019, **23**, 367-374.
14. W. Zhang, W. K. Pang, V. Sencadas and Z. Guo, *Joule*, 2018, **2**, 1534-1547.
15. W. Miao, X. Zhao, R. Wang, Y. Liu, L. Li, Z. Zhang and W. Zhang, *J. Colloid Interf. Sci.*, 2019, **556**, 432-440.
16. Z. Zhang, C. Wu, Z. Chen, H. Li, H. Cao, X. Luo, Z. Fang and Y. Zhu, *J. Mater. Chem. A*, 2020, **8**, 3369-3378.
17. X. Wu, W. Zhao, H. Wang, X. Qi, Z. Xing, Q. Zhuang and Z. Ju, *J. Power Sources*, 2018, **378**, 460-467.
18. W. Zhang, J. Mao, S. Li, Z. Chen and Z. Guo, *J. Am. Chem. Soc.*, 2017, **139**, 3316-3319.
19. W. C. Chang, J. H. Wu, K. T. Chen and H. Y. Tuan, *Adv. Sci.*, 2019, **6**, 1801354.
20. Y. Wu, S. Hu, R. Xu, J. Wang, Z. Peng, Q. Zhang and Y. Yu, *Nano Lett.*, 2019, **19**, 1351-1358.
21. P. Xiong, P. Bai, S. Tu, M. Cheng, J. Zhang, J. Sun and Y. Xu, *Small*, 2018, **14**, 1802140.
22. W. Zhang, Z. Wu, J. Zhang, G. Liu, N. Yang, R. Liu, W. K. Pang, W. Li and Z. Guo, *Nano Energy*, 2018, **53**, 967-974.
23. Y. Yi, W. Zhao, Z. Zeng, C. Wei, C. Lu, Y. Shao, W. Guo, S. Dou and J. Sun, *Small*, 2020, **16**, 1906566.
24. X. Huang, X. Sui, W. Ji, Y. Wang, D. Qu and J. Chen, *J. Mater. Chem. A*, 2020, **8**, 7641-7646.